

Robust error bounds for quantised and pruned neural networks

Jiaqi Li

Ross Drummond

Stephen R. Duncan

JIAQI.LI@ST-HUGHS.OX.AC.UK

ROSS.DRUMMOND@ENG.OX.AC.UK

STEPHEN.DUNCAN@ENG.OX.AC.UK

Department of Engineering Science, University of Oxford, 17 Parks Road, OX1 3PJ, Oxford, United Kingdom

Abstract

With the rise of smartphones and the internet-of-things, data is increasingly getting generated at the edge on local, personal devices. For privacy, latency and energy saving reasons, this shift is causing machine learning algorithms to move towards a decentralised approach, with the data and algorithms stored and even trained locally on devices. The device hardware becomes the main bottleneck for model performance in this set-up, creating a need for slimmed down, more efficient neural networks. Neural network pruning and quantisation are two methods that have been developed to achieve this, with both approaches demonstrating impressive results in reducing the computational cost without sacrificing too much on model performance. However, our understanding behind these methods remains underdeveloped. To address this issue, a semi-definite program to robustly bound the error caused by pruning and quantising a neural network is introduced in this paper. The method can be applied to generic neural networks, accounts for the many non-linearities of the problem and holds robustly for all inputs in specified sets. It is hoped that the computed bounds will give certainty to software/control/machine learning engineers implementing these algorithms efficiently on limited hardware.

Keywords: Robustness; quantised neural networks; error bounds.

1. Introduction

The way we generate data is rapidly changing in light of the rise of the internet-of-things and the widespread use of smartphones (Zhou et al., 2019). In terms of data sources, there is an accelerating shift away from big data, like e-commerce records, stored on mega-scale cloud data centres towards more localised data sources generated by users interacting with their personal devices (Zhang et al., 2019). This evolving data landscape is causing a rethink to how machine learning algorithms are trained and implemented.

The most intuitive way to train and implement these algorithms within this new data landscape remains *centralised learning* where the data is sent to a central data centre in the cloud upon which the algorithm is then trained and run (Zhou et al., 2019). This approach should give the best model performance and is a natural extension of existing algorithm training frameworks but has several flaws (Zhou et al., 2019; Gündüz et al., 2019). These include 1. Concerns around user privacy since the data is stored in a data centre owned by a third party, 2. The increased latency of centralised algorithms to respond to new data, 3. As the algorithms get ever larger in response to the growing availability of data, they are requiring significantly more compute power, memory storage and energy.

These flaws are inherent to centralised learning and are leading growing efforts to direct machine learning towards a more *decentralised* approach. With decentralised learning (Zhang et al., 2019; Zhou et al., 2019) (often known as *edge intelligence* (Zhou et al., 2019; Deng et al., 2020; Shi et al.,

2020) and falling under the umbrella of *distributed learning* (Zhang et al., 2019) amongst other labels), there is a greater emphasis on implementing and even training the algorithms locally on devices. In this way, decentralised learning aims to generate smaller, more personalised algorithms that can help circumnavigate the above mentioned issues with centralised learning- albeit typically doing so at the expense of model performance (Zhang et al., 2019). Running the algorithms locally on the devices means that hardware constraints (e.g. memory availability, compute power and energy consumption) are important. Managing these constraints whilst still delivering reasonable model performance is one of the main bottlenecks that decentralised learning needs to overcome, and has led to a push for slimmed-down, efficient algorithms (typically neural networks (NNs)- the class of model focussed on in this work). As such, there has been increased interest in pruned neural networks which sparsify the weights and biases (Blalock et al., 2020) and quantised neural networks (e.g. (Shin et al., 2016; Courbariaux et al., 2014; Sung et al., 2015)) which use a coarse fixed-point representation of the algorithm’s parameters. However, a full and robust understanding of how modifications like network pruning and quantisation affect the neural networks outputs, that goes beyond sensitivity studies like (Shin et al., 2016) for instance, is as yet still not fully developed.

To address these issues, this paper provides performance guarantees for implementing neural networks on low-cost and memory-limited hardware. Specifically, we address the problem of determining how the output of a neural network is corrupted by quantising the model’s parameters and the data by storing them using fixed-point arithmetic or from pruning. In other words, bounds for quantised and pruned neural networks are introduced. The main contributions are:

- A semi-definite program (SDP) is introduced to robustly bound the error from pruning and storing a neural network’s weights, biases and input using fixed-point arithmetic. In other words, robust error bounds for pruned and quantised neural networks are introduced.
- The proposed bounds hold robustly for all input data in specified sets, accounts for the neural network’s nonlinearities and are generated from a convex semi-definite programmes.
- The neural network quantisation bounds are shown to be special cases of a more general problem, called the neural network similarity problem, which bounds the worst-case error of two different neural networks outputs for all inputs in some specific sets.
- The application of the bounds are explored in several numerical examples.

This result allows us to guarantee the worst-case error following from the corruption of a trained neural network by pruning it or implementing it on low-cost, memory-limited hardware with fixed-point arithmetic, as in for quantised neural networks. To arrive at this bound, a more general problem is first introduced in Problem 1 that bounds the worst-case error between the outputs of two generic neural networks. This general problem is labelled the neural network *similarity problem* and draws heavily from the notion of incremental stability in dynamical systems (Zames, 1966). By setting the second NN of this problem to be a quantised or pruned NN, the desired error bounds are obtained as a special case.

Related work: Many results have demonstrated the potential of both quantised and pruned neural networks to realise machine learning on limited hardware. For example, Gong et al. (2014) achieved a 16-24 \times network compression for the 1000-category classification on the ImageNet challenge with only a 1% loss of classification accuracy and Lin et al. (2016) showed no loss in accuracy by reducing a model trained on the CIFAR-10 benchmark by $> 20\%$. More extreme levels of quantisation

have also been explored, for example with binarised neural networks (where the weights and/or activation functions are restricted to be binary) which have also demonstrated, e.g. in [Hubara et al. \(2016\)](#) and [Rastegari et al. \(2016\)](#), rapid compute speeds and large memory savings without significant accuracy losses.

The quantisation error bounds presented in this work are closely related to the semi-definite programmes for certifying neural network robustness developed in [Fazlyab et al. \(2019\)](#); [Raghunathan et al. \(2018\)](#); [Dathathri et al. \(2020\)](#). These SDPs guarantee that small perturbations in the input will not lead to large variations in the NN output and can help prevent against adversarial attacks and make the NNs more reliable to out-of-sample data. Recently, there has been a focus on the scalability of these SDP robustness certificates ([Dathathri et al., 2020](#)) (since they scale by $\mathcal{O}(n^6)$ in runtime and $\mathcal{O}(n^4)$ in memory requirements, where n is the number of neurons in the network ([Dathathri et al., 2020](#))), a particularly exciting direction for this paper as it could help make the presented bounds applicable to larger NNs.

Acronyms, Notations and Preliminaries

\mathbb{R}_+ , \mathbb{R}_+^n and $\mathbb{R}_+^{n \times n}$ denote real non-negative numbers, non-negative real vectors of dimension n and real non-negative matrices of size $n \times n$ respectively. Non-negative diagonal matrices of size $n \times n$ are denoted \mathbb{D}_+^n . \mathbb{Z}_+ (\mathbb{Z}_-) is the set of positive (negative) integers. The set of natural numbers (non-negative integers) is \mathbb{N} . The matrix of zeros of dimension $n \times m$ is $\mathbf{0}_{n \times m}$ and $\mathbf{0}_n$ is the vector of zeros of dimension n . The matrix of ones of dimension $N \times M$ is $\mathbf{1}_{N \times M}$ and $\mathbf{1}_N$ is the vector of ones of dimension N . The i^{th} element of a vector x is denoted x_i unless otherwise defined in the text. Strict and element-wise LMIs are posed as $F(x) > 0$ while nonstrict and element-wise LMIs are written as $F(x) \geq 0$. A positive (negative) definite matrix Ω is denoted $\Omega \succ (\prec) 0$, and a positive (negative) semi-definite Γ matrix is written $\Gamma \succeq (\preceq) 0$. The p -norm is displayed by $\|\cdot\|_p : \mathbb{R}^n \rightarrow \mathbb{R}_+$, $p \in \mathbb{N}$. Where acronyms are used, “NN” stands for “artificial neural network”, “QC” stands for quadratic constraint, “LMI” stands for “linear matrix inequality”, and “SDP” stands for “semi-definite programme”.

2. Neural Networks: Representation in state-space form

Consider two functions $f_1(x_1) : \mathcal{X} \rightarrow \mathcal{F}$ and $f_2(x_2) : \mathcal{X} \rightarrow \mathcal{F}$ acting upon input data $x_1, x_2 \in \mathcal{X}$. These functions are assumed to be defined by feed-forward NNs composed of ℓ hidden layers, with the k^{th} layer composed of n_k neurons and the total number of neurons being $N = \sum_{k=1}^{\ell} n_k$. Both the first

$$x_1^0 = x_1, \tag{1a}$$

$$x_1^{k+1} = \phi(W_1^k x_1^k + b_1^k), \quad k = 0, 1, \dots, \ell - 1, \tag{1b}$$

$$f_1(x_1) = W_1^\ell x_1^\ell + b_1^\ell, \tag{1c}$$

and second neural network

$$x_2^0 = x_2, \tag{2a}$$

$$x_2^{k+1} = \phi(W_2^k x_2^k + b_2^k), \quad k = 0, 1, \dots, \ell - 1, \tag{2b}$$

$$f_2(x_2) = W_2^\ell x_2^\ell + b_2^\ell, \tag{2c}$$

can be expanded out in the above state-space-like form. Here, for neural network $i \in \{1, 2\}$, $x_i^0 \in \mathcal{X}_i \subseteq \mathbb{R}^{n_x}$ represents the input data, $W_i^k \in \mathbb{R}^{n_{k+1} \times n_k}$ the weights, $b_i^k \in \mathbb{R}^{n_{k+1}}$ the biases, $k = 0, \dots, \ell - 1$, defines the network layers, n_x and n_f are, respectively, the network's input and output dimensions and $\phi(\cdot)$ are the activation functions- typically a rectified Linear Unit (ReLU), sigmoid or tanh- but in this paper can be any function satisfying some of the properties of Definition 4 in Appendix 4. These activation function will be taken to act element-wise on their vector arguments.

2.1. A compact neural network representation

For the $i^{\text{th}} \in \{1, 2\}$ neural network, define the arguments of nonlinear activation functions $\phi(\cdot)$ as

$$\xi_i = \begin{bmatrix} \xi_i^1 \\ \xi_i^2 \\ \vdots \\ \xi_i^\ell \end{bmatrix} = \begin{bmatrix} W_i^0 & \mathbf{0}_{n_1 \times n_1} & \cdots & \mathbf{0}_{n_1 \times n_{\ell-1}} \\ \mathbf{0}_{n_2 \times n_2} & \ddots & \ddots & \vdots \\ \vdots & \ddots & \ddots & \mathbf{0}_{n_{\ell-1} \times n_{\ell-2}} \\ \mathbf{0}_{n_\ell \times n_x} & \cdots & \mathbf{0}_{n_1 \times n_{\ell-2}} & W_i^{\ell-1} \end{bmatrix} \begin{bmatrix} x_i^0 \\ x_i^1 \\ \vdots \\ x_i^{\ell-1} \end{bmatrix} + \begin{bmatrix} b_i^0 \\ b_i^1 \\ \vdots \\ b_i^{\ell-1} \end{bmatrix} \in \mathbb{R}^M. \quad (3)$$

These vectors allow the i^{th} NN of (1) and (2) to be written in the more compact form

$$\xi_i^k = W_i^k x_i + b_i^k, \quad k = 0, 1, \dots, \ell - 1, \quad (4a)$$

$$x_i^{k+1} = \phi(\xi_i^k), \quad k = 0, 1, \dots, \ell - 1, \quad (4b)$$

$$f_i(x_i) = W_i^\ell \phi(\xi_i^\ell) + b_i^\ell. \quad (4c)$$

The vectors

$$\mu = [\xi_1^T, \xi_2^T, \phi(\xi_1)^T, \phi(\xi_2)^T, 1]^T, \eta = [x_1^T, x_2^T, \phi(\xi_1)^T, \phi(\xi_2)^T, 1]^T, \quad (5)$$

will also be used throughout the paper to build the various inequalities. These two vectors are linearly related through a matrix $E \in \mathbb{R}^{2(n_x+M)+1 \times 4M+1}$ by

$$\eta = E\mu. \quad (6)$$

2.2. The neural network similarity problem: Bounding the worst-case error between two neural networks

The neural network *similarity problem* is now introduced to bound the worst-case error between the outputs of two neural networks for all input data in some sets. As such, the solutions to this problem indicates how similar two NNs are to each other in a worst-case setting. Figure. 3 in Appendix 1 illustrates the general idea behind this problem.

Problem 1 Given two neural networks $f(x_1) : \mathcal{X} \rightarrow \mathcal{F}$ and $f(x_2) : \mathcal{X} \rightarrow \mathcal{F}$ defined by (1) and (2) with inputs $(x_1, x_2) \in \mathcal{X}$, find the smallest $(\gamma_x, \gamma_{x_1}, \gamma_{x_2}, \gamma) \in \mathbb{R}_+$ such that for some $(p, q_{x_1}, q_{x_2}, q) \in \mathbb{N}$, the following bound holds

$$\|f_1(x_1) - f_2(x_2)\|_p \leq \gamma_{x_1} \|x_1\|_{q_{x_1}} + \gamma_{x_2} \|x_2\|_{q_{x_2}} + \gamma_x \|x_1 - x_2\|_q + \gamma, \quad \forall x_1, x_2 \in \mathcal{X}. \quad (7)$$

The reason for introducing the above problem is that it provides the general framework to address the specific problem of interest to this paper- that of bounding the worst-case error of a pruned or quantised neural network. To specialise Problem 1 to the computation of this NN quantisation bound, the second neural network in Problem 1 set to be the quantised one, as in

$$W_2^k = q(W_1^k), \quad b_2^k = q(b_1^k), \quad x_2 = q(x_1), \quad (8)$$

where $q(\cdot)$ is the quantisation function defined in Section 3.2. Likewise for pruned NNs, the second NN is set to be the pruned one.

Computing tractable solutions to the neural network collaboration problem is the main focus of the remaining sections of this paper. And whilst this work focusses on bounding the quantisation error in neural networks, future work will explore applying Problem. 1 to compute other robust bounds for neural networks, such as quantifying the impact of network pruning.

3. Quantised neural networks

With the neural network collaboration problem for bounding the error between two different neural networks introduced, this section outlines the mathematical representation of quantised neural networks.

3.1. Fixed-point arithmetic

It will be assumed that the quantised neural network’s weights, biases and data are stored using fixed-point arithmetic. The $\langle \text{IB}, \text{FB} \rangle$ format for fixed-point representations adopted in Gupta et al. (2015); Holi and Hwang (1993) will be used, whereby IB and FB respectively denote the number of bits allocated for the integer and fractional parts of the number. Figure 1 illustrates how this number representation is used, showing the 8-bit fixed-point representation of the number 31.4592 with the equation for this conversion between a fix-point binary format and a decimal number described in Appendix. 2. In this work, saturation of the representation is neglected. This is an important issue but could be avoided with the introduction of “temporary fixed-point registers with enough number of bits” (Gupta et al. (2015)).

3.2. Quantisation function

The piece-wise constant quantisation function $q(\cdot)$ acting element-wise on vector and matrix arguments can be used to capture the fixed-point representation of the quantised neural network’s weights, biases and data, as illustrated in Figure. 1.

Given a real number $s \in \mathbb{R}$, the quantisation function is defined as

$$q(s) \triangleq \frac{\text{sgn}(s) \lfloor |s| \cdot \Delta \rfloor}{\Delta}, \Delta = 2^{-\text{FB}}, \text{FB} \in \mathbb{N}. \quad (9)$$

when $\lfloor \cdot \rfloor$ is the ‘floor’ operator and Δ is the binary quantisation step, with the word length FB setting the numerical precision of the quantisation. Decreasing FB causes a coarse fixed-point representation, resulting in information being lost because of the quantisation and the neural network’s output being corrupted, inducing an error.

Note in this work the floor rounding scheme was used, i.e. $q(\cdot)$ maps an input value to the largest integer multiple of Δ smaller than the input value. Other rounding schemes exist and may

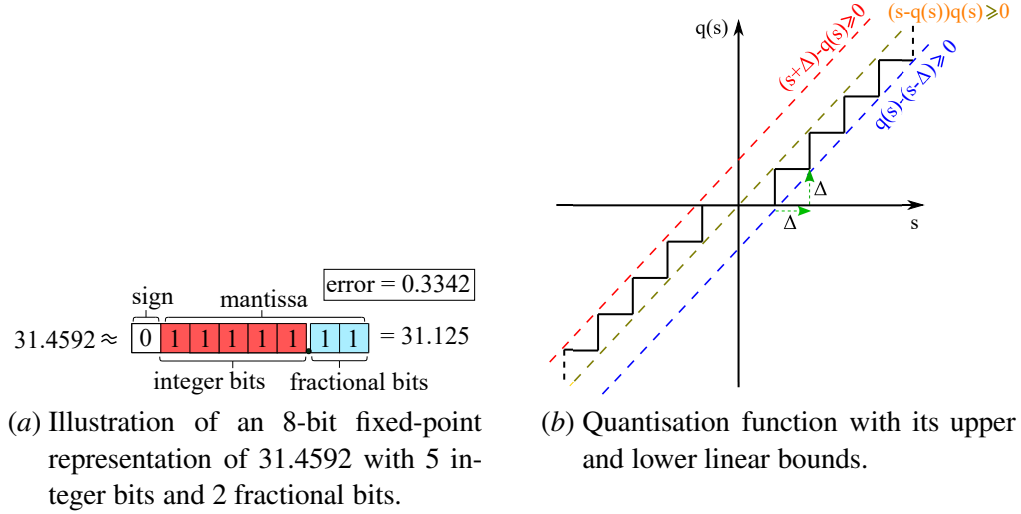


Figure 1: Illustrations of the 8-bit fixed-point representation of 31.4592 and the quantisation function used to represent the number discretisation in the analysis.

be adapted into the proposed framework, e.g. round-to-nearest (Gupta et al. (2015)) and various piece-wise-linear and stochastic rounding methods.

As ReLU activation functions were adopted for the numerical results of this paper, the effect of additionally quantising these functions was ignored. However, this effect could be incorporated into the analysis as long as the quantised activation functions satisfy the quadratic constraints.

4. Abstracting the nonlinearities and sets using quadratic constraints

In general, solving Problem 1 is intractable because of a) the non-convex mapping of each NN with nonlinear activation functions and b) the bounds are required to hold robustly for all inputs in $(x_1, x_2) \in \mathcal{X}$ with \mathcal{X} allowed to be infinite dimensional. Using quadratic constraints, this paper is able to provide an upper bound by producing an algebraic, convex outer-approximation of the various sets and nonlinearities of the problem. This allows solutions to Problem 1 to be computed via a SDP, with the conservatism of the approach coming from the fact that it only implicitly characterises the various nonlinearities and sets of the analysis. A brief overview of quadratic constraints can be found in Appendix 3. The remaining part of this section details the quadratic constraints of the problem that describe the input set (Appendix 4) and its quantisation (Appendix 6), activation functions (Appendix 5), and the error bound (15).

4.1. Abstraction of the input set

The various quadratic constraints satisfied when the NN inputs are contained to the set $(x_1, x_2) \in \mathcal{X}$ are detailed in Appendix 4. If these constraints are satisfied, then whenever $(x_1, x_2) \in \mathcal{X}$, there exists a matrix $P_{\mathcal{X}} \in \mathbb{R}^{2(n_x+M)+1 \times 2(n_x+M)+1}$ built from the matrix variables (the lambdas of Definition 3 in Appendix 4) such that

$$M_{\mathcal{X}}(P_{\mathcal{X}}) = \eta^T P_{\mathcal{X}} \eta \geq 0, \quad \forall (x_1, x_2) \in \mathcal{X}. \quad (10)$$

4.2. Abstraction of the activation functions

Dealing with the nonlinear activation functions is the main source of difficulty in generating robust solutions to Problem 1. Thankfully, most of the commonly used NN activation functions (e.g. those mentioned in Table. 1 in Appendix 4) have properties that allow them to be characterised by quadratic constraints (Drummond et al., 2020). The mathematical definitions for these properties can be found in Definition. 4 of Appendix 5 and the associated quadratic constraints are given in Lemma. 5 of Appendix 5.

Using the compact NN representation of (4), the various quadratic constraints satisfied by the activation function in Lemma. 5 in Appendix 5 can be collected together and represented as a single inequality

$$M_\phi(\Lambda) = \mu^T \Lambda \mu = \eta^T (E^T \Lambda E) \eta \geq 0, \quad \forall (x_1, x_2) \in \mathcal{X}, \quad (11)$$

with the matrix

$$\Lambda = \begin{bmatrix} \mathbf{0}_{N \times N} & \mathbf{0}_{N \times N} & \Lambda_{13} & \Lambda_{14} & \Lambda_{15} \\ \mathbf{0}_{N \times N} & \mathbf{0}_{N \times N} & \Lambda_{23} & \Lambda_{24} & \Lambda_{25} \\ \Lambda_{13}^T & \Lambda_{23}^T & \Lambda_{33} & \Lambda_{34} & \Lambda_{35} \\ \Lambda_{14}^T & \Lambda_{24}^T & \Lambda_{34}^T & \Lambda_{44} & \Lambda_{45} \\ \Lambda_{15}^T & \Lambda_{25}^T & \Lambda_{35}^T & \Lambda_{45}^T & \Lambda_{55} \end{bmatrix} \quad (12)$$

composed from $\Lambda_{i,j}, \{i, j\} \in \{1, 2, 3, 4, 5\}$ being linear combinations of the scaling variables of the various quadratic constraints of $\phi(\cdot)$, e.g. the lambdas of Lemma 5 in Appendix 5.

4.3. Abstraction of the quantisation function

Besides the activation functions $\phi(\cdot)$, for quantised NNs the quantisation function $q(x_i)$ from (9) acting on the input data is another nonlinearity that will have to be accounted for in the analysis if the error bounds are to be obtained. Thankfully, this nonlinear function also satisfies certain quadratic constraints as defined in Lemma 7 of Appendix 6. These quadratic constraints for the quantisation function can then be combined into the single inequality

$$M_q(P_q) = \eta^T P_q \eta \geq 0, \quad \forall (x_1, x_2) \in \mathcal{X}, \quad (13)$$

for some matrix variable P_q built from the various lambdas of Lemma 7.

4.4. Abstraction of the comparison error

A quadratic upper bound for the comparison error between the two networks is used as the performance metric for the problem

$$\|f_1(x_1) - f_2(x_2)\|_2^2 \leq \gamma_{x_1} \|x_1\|_2^2 + \gamma_{x_2} \|x_2\|_2^2 + \gamma_x \|x_1 - x_2\|_2^2 + \gamma, \quad \gamma_x \geq 0, \gamma \geq 0. \quad (14)$$

This metric can be equivalently expressed as the quadratic

$$M_{\|f-g\|_2}(\Gamma) = \eta^T \Gamma(\gamma_{x_1} \gamma_{x_2}, \gamma_x, \gamma) \eta \leq 0, \quad \forall (x_1, x_2) \in \mathcal{X}. \quad (15)$$

With respect to the metric defined in (7) of Problem 1, (14) uses the squared 2-norm ($p = q = 2$). The main advantage of using the 2-norm in this context is that the error bounds can be computed from the solution of a SDP, with its main drawback being that the ∞ -norm is normally preferred for machine learning applications. However, the computational advantages of the quadratic 2-norm justified its use here.

5. Neural network comparison bounds as a semidefinite programme

With the QCs defined for each feature of the problem, upper bounds to (14) can now be computed from the following SDP. Again, this result is posed in the general setting of solving Problem 1, with the specialisation to robust error bounds for quantised neural networks obtained by including the quantisation quadratic constraints of (13) into the linear matrix inequality of (16b).

Theorem 1 *Consider the two neural networks of (1) and (2) satisfying the quadratic constraints of (10), (11) and (13). Set the weights $(w_{x_1}, w_{x_2}, w_x, w_{aff}) \in \mathbb{R}_+$ scaling the relative importance of the quadratic and affine terms in the error bound (14). If there exists a solution to*

$$\min \quad w_{x_1}\gamma_{x_1} + w_{x_2}\gamma_{x_2} + w_x\gamma_x + w_{affine}\gamma, \quad (16a)$$

$$\text{subject to} \quad P_{\mathcal{X}}(\cdot) + P_q(\cdot) + E^T \Lambda(\cdot) E + \Gamma(\cdot) \prec 0, \quad (16b)$$

$$\gamma_{x_1} \geq 0, \gamma_{x_2} \geq 0, \gamma_x \geq 0, \gamma \geq 0. \quad (16c)$$

with the matrix variables $P_{\mathcal{X}}(\cdot)$, $P_q(\cdot)$, $\Lambda(\cdot)$ and $\Gamma(\cdot)$ defined in (10), (13), (11) and (15), then the comparison error is bounded from above by

$$\|f_1(x_1) - f_2(x_2)\|_2^2 < \gamma_{x_1}\|x_1\|_2^2 + \gamma_{x_2}\|x_2\|_2^2 + \gamma_x\|x_1 - x_2\|_2^2 + \gamma, \quad (x_1, x_2) \in \mathcal{X}. \quad (17)$$

Proof See Appendix 7. ■

6. Numerical examples and discussion

In this section, the effectiveness of the obtained bounds was explored with several numerical examples. The first subsection presents examples for bounding the comparison error between two generic neural networks, and the second is focused on quantised and pruned networks.

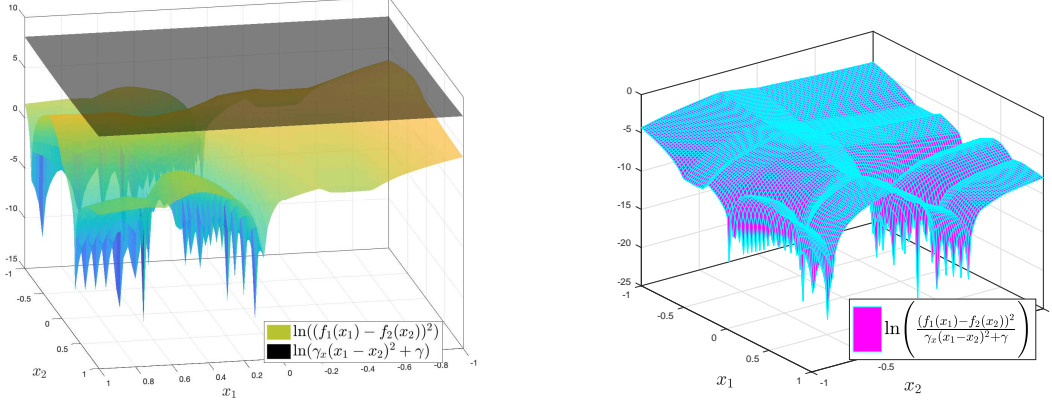
In all the examples, the input was constrained to the hyper-cube $(x_1, x_2) \in \mathcal{X} = \{x_1, x_2 \in \mathbb{R}^{n_x} \mid |x_1|, |x_2| \leq \bar{x}\}$, where $\bar{x} = 1$ and the ReLU was chosen as the activation function. The SDP of Theorem 5, applied to the neural network similarity problem and the quantised network problem, was solved using the MOSEK (ApS, 2019) solver implemented through the YALMIP (Löfberg, 2004) interface of MATLAB. The code and the various models used in the examples can be found at <https://github.com/ElrondL/Robust-Quantisation-Bounds>.

6.1. Neural network comparison performance

For the first experiment, the performance of the framework defined in Theorem 5 and Definition 6 in Appendix 5 was checked by comparing randomly generated neural networks with $n_x = 1$ as the input dimension, $n_f = 1$ as the output dimension and $\ell = \{1, 2, 3, 4\}$ hidden layers, each with $n_k = 10$ neurons. The two neural networks were fed with randomly generated signals $\{x_1, x_2\} \in \mathcal{X}$. For each NN layer dimension (ℓ), 100 random neural networks were generated and the average γ_x , γ , mean bound tightness, maximum bound tightness, minimum bound tightness, and runtime (in seconds) were recorded. Tightness of the bound was defined as the natural log error between the output difference norm and the over approximation bound

$$T = \ln((f(x_1) - f(x_2))^2) - \ln(\gamma_x(x_1 - x_2)^2 + \gamma), \quad (18)$$

with the results given in Table 2 of Appendix 8.



(a) The error (coloured) and bound (grey) surfaces.

(b) The tightness surface T of the bound and error surfaces in Fig.2(a), viewed from another angle.

Figure 2: Example neural network comparison bound with $\ell = 3$.

A bounding surface holding robustly for all inputs generated was obtained for each test case, an example of which can be found in Figure 2. It was observed that when $n_x = 1$ and $n_f = 1$, the bound was relatively tight (i.e. $T \leq 3.5$) for the majority of the input space. In cases where the error was extremely small, the distance between the bound and the error surface was large. It was observed that the distance between the bound and the error surface became larger with an increasing number of neurons and for multi-dimensional input and output vectors, as reflected in Table 2’s data.

6.2. Quantisation error bound

Error bounds were also computed for quantised NNs where $W_2 = q(W_1)$, $b_2 = q(b_1)$ and $x_2 = q(x_1)$. Here, the output dimension was $n_f = 1$, the input dimension was $n_x = 1$ with the input set for x_1 consisting of 100 evenly spaced values in $[-1, 1]$. The quantisation step was $\Delta = 2^{-3}$. Figure 4 in Appendix 8 contains typical error bound curves for the various models considered and also an example in 3D (where the condition $x_2 = q(x_1)$ was relaxed, giving a looser bound as the input space was less restricted).

For each group of NNs with ℓ hidden layers, 100 random NNs were generated with the corresponding results shown in Table 3 of Appendix 8. Also, for quantisation levels $\Delta = 2^i$, $i \in \{1, 2, 3, 4, 5\}$, 100 random neural networks with $\ell = 2$ were generated with the results shown in Table 4 of Appendix 8. Bound tightness was defined as the natural log error between the original and quantised networks’ output difference norm and the over-approximation bound

$$T_q = \ln(f(x_1) - f_2(x_2)^2) - \ln(\gamma_x(x_1)^2 + \gamma). \quad (19)$$

A bounded curve that held robustly for all inputs was generated for each test case, with the step patterns of the error curves following from the quantisation. It was also observed that the bound loosened with an increasing number of neurons, as seen in Table 3 of Appendix 8.

Worst case quantisation error bound

The worst-case quantisation error and bound values were also recorded and averaged for 100 random neural networks of $\ell = 2$ layers for quantisation levels $\Delta = 2^i, i \in \{1, 2, 3, 4, 5\}$. Note that the bound and error values come in pairs, so there exists a bound value corresponding with the maximum error as well as an error value corresponding to the maximum bound value. The averages of both the bound and error were also recorded. These results were then plotted in Figure 5 of Appendix 8. The maximum bound values tended to be close to the observed maximum error however the gap between the corresponding maximum error and the bound tended to be quite large. It was also observed that both the error and bound decreased with an increasing level of quantisation, and they did so at similar rates.

Pruned neural networks

The proposed framework could also be used to bound the comparison error between a randomly-generated 40-neuron neural network and its pruned version (with $f_x(x_2)$ in Problem 1 being the pruned one), where the weights of the eight hidden neurons with the smallest 2-norms were set to zero (Blalock et al. (2020)). Note, that by setting the second neural network to be identical to the first, our framework could also bound the behaviour of a neural network within to its input space. Pruning that removes neurons rather than setting weights to zero could also be bounded with this framework. Figure 6 in Appendix 8 shows the results for the pruned network with the computed bound.

Conclusions

A method to generate upper bounds for the error induced by either quantising or pruning a trained neural network was introduced. The method's bound were shown to hold robustly for all inputs in pre-specified sets, account for the models nonlinearities and was generated from the solution of a semi-definite programme. The computed bounds were evaluated in several numerical examples, showcasing their validity. Future work will explore reducing the conservatism of the bounds, improving the scalability of the semi-definite programming solvers and applying the method to other problems of interest where the similarity of two neural networks is to be evaluated.

Acknowledgments

Ross Drummond would like to thank the Royal Academy of Engineering for funding this research through a UKIC Fellowship as well as the Nextrode project of the Faraday Institution. Jiaqi Li would like to thank the Department of Engineering, University of Oxford for funding through the UROP placement scheme.

References

- MOSEK ApS. *The MOSEK optimization toolbox for MATLAB manual. Version 9.0.*, 2019. URL <http://docs.mosek.com/9.0/toolbox/index.html>.
- Davis Blalock, Jose Javier Gonzalez Ortiz, Jonathan Frankle, and John Gutttag. What is the state of neural network pruning? *arXiv preprint arXiv:2003.03033*, 2020.
- Matthieu Courbariaux, Yoshua Bengio, and Jean-Pierre David. Training deep neural networks with low precision multiplications. *arXiv preprint arXiv:1412.7024*, 2014.
- Sumanth Dathathri, Krishnamurthy Dvijotham, Alexey Kurakin, Aditi Raghunathan, Jonathan Uesato, Rudy R Bunel, Shreya Shankar, Jacob Steinhardt, Ian Goodfellow, Percy S Liang, et al. Enabling certification of verification-agnostic networks via memory-efficient semidefinite programming. *Advances in Neural Information Processing Systems*, 33, 2020.
- Shuiguang Deng, Hailiang Zhao, Weijia Fang, Jianwei Yin, Schahram Dustdar, and Albert Y Zomaya. Edge intelligence: the confluence of edge computing and artificial intelligence. *IEEE Internet of Things Journal*, 2020.
- Ross Drummond, C. Turner Turner, and Stephen R. Duncan. Reduced-order neural network synthesis with robustness guarantees. *Under review in the IEEE Transactions on Neural Networks and Learning Systems*, 2020.
- Mahyar Fazlyab, Manfred Morari, and George J Pappas. Safety verification and robustness analysis of neural networks via quadratic constraints and semidefinite programming. *arXiv preprint arXiv:1903.01287*, 2019.
- Yunchao Gong, Liu Liu, Ming Yang, and Lubomir Bourdev. Compressing deep convolutional networks using vector quantization. *arXiv preprint arXiv:1412.6115*, 2014.
- Deniz Gündüz, Paul de Kerret, Nicholas D Sidiropoulos, David Gesbert, Chandra R Murthy, and Mihaela van der Schaar. Machine learning in the air. *IEEE Journal on Selected Areas in Communications*, 37(10):2184–2199, 2019.
- Suyog Gupta, Ankur Agrawal, Kailash Gopalakrishnan, and Pritish Narayanan. Deep learning with limited numerical precision. *CoRR*, abs/1502.02551, 2015. URL <http://arxiv.org/abs/1502.02551>.
- J. L. Holi and J. . Hwang. Finite precision error analysis of neural network hardware implementations. *IEEE Transactions on Computers*, 42(3):281–290, 1993. doi: 10.1109/12.210171.
- Itay Hubara, Matthieu Courbariaux, Daniel Soudry, Ran El-Yaniv, and Yoshua Bengio. Binarized neural networks. In *Advances in neural information processing systems*, pages 4107–4115, 2016.
- Ulf Jönsson. Lecture notes on integral quadratic constraints. 2001.
- Darryl Lin, Sachin Talathi, and Sreekanth Annapureddy. Fixed point quantization of deep convolutional networks. In *International conference on machine learning*, pages 2849–2858, 2016.
- J. Löfberg. Yalmip : A toolbox for modeling and optimization in matlab. In *In Proceedings of the CACSD Conference*, Taipei, Taiwan, 2004.

- Aditi Raghunathan, Jacob Steinhardt, and Percy S Liang. Semidefinite relaxations for certifying robustness to adversarial examples. In *Advances in Neural Information Processing Systems*, pages 10877–10887, 2018.
- Mohammad Rastegari, Vicente Ordonez, Joseph Redmon, and Ali Farhadi. Xnor-net: Imagenet classification using binary convolutional neural networks. In *European conference on computer vision*, pages 525–542. Springer, 2016.
- Yuanming Shi, Kai Yang, Tao Jiang, Jun Zhang, and Khaled B Letaief. Communication-efficient edge ai: Algorithms and systems. *arXiv preprint arXiv:2002.09668*, 2020.
- Sungho Shin, Kyuyeon Hwang, and Wonyong Sung. Fixed-point performance analysis of recurrent neural networks. In *2016 IEEE International Conference on Acoustics, Speech and Signal Processing (ICASSP)*, pages 976–980. IEEE, 2016.
- Wonyong Sung, Sungho Shin, and Kyuyeon Hwang. Resiliency of deep neural networks under quantization. *arXiv preprint arXiv:1511.06488*, 2015.
- Sophie Tarbouriech, Germain Garcia, João Manoel Gomes da Silva Jr, and Isabelle Queinnec. *Stability and stabilization of linear systems with saturating actuators*. Springer Science & Business Media, 2011.
- George Zames. On the input-output stability of time-varying nonlinear feedback systems part one: Conditions derived using concepts of loop gain, conicity, and positivity. *IEEE Transactions on Automatic Control*, 11(2):228–238, 1966.
- Chaoyun Zhang, Paul Patras, and Hamed Haddadi. Deep learning in mobile and wireless networking: A survey. *IEEE Communications Surveys & Tutorials*, 21(3):2224–2287, 2019.
- Bin Zhou, Guang-Ren Duan, and James Lam. On the absolute stability approach to quantized feedback control. *Automatica*, 46(2):337–346, 2010.
- Zhi Zhou, Xu Chen, En Li, Liekang Zeng, Ke Luo, and Junshan Zhang. Edge intelligence: Paving the last mile of artificial intelligence with edge computing. *Proceedings of the IEEE*, 107(8): 1738–1762, 2019.

Appendices

Appendix 1: Illustration of the neural network similarity problem

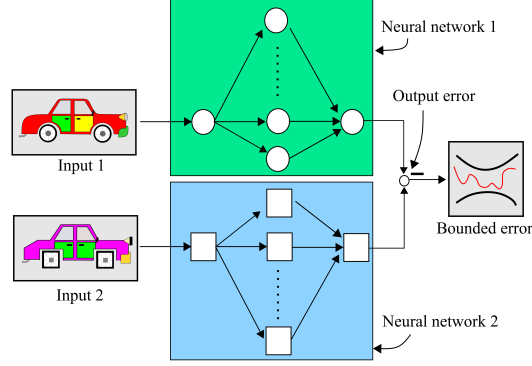


Figure 3: Illustration of the similarity problem which bounds the worst case error between the outputs of two neural networks for all inputs in some set $(x_1, x_2) \in \mathcal{X}$. By setting the second neural network in this set-up to be the quantised or pruned one, the desired error bounds can be computed.

Appendix 2: Representing numbers with fixed-point arithmetic

Given a binary number (BN) represented in fixed-point format, the original decimal format (DN) can be recovered from

$$DN = \sum_{i=1}^{IB-1} BN_{\langle I \rangle_i} * 2^i + \sum_{j=1}^{FB-1} BN_{\langle F \rangle_j} * 2^{-j}, \quad (20)$$

with $\langle I \rangle$ and $\langle F \rangle$ denoting the integer and fractional parts of BN .

Appendix 3: Quadratic constraints overview

As suggested by their name, a quadratic constraint is simply a non-negative quadratic algebraic expression capturing dependencies between its arguments. For instance, the following is satisfied by the ReLU nonlinearity

$$p_i(s, \sigma) = (s - \text{ReLU}(s))\sigma \geq 0, \quad \forall (s, \sigma) \in \mathbb{R}. \quad (21)$$

Now, consider the case where we have N quadratic constraints $p_i(\cdot) \geq 0$ for $i = 1, \dots, N$ mapping $\mathbb{R}^n \rightarrow \mathbb{R}_+$ but want to show the negativity of another $p_0(s, \sigma) < 0$. This is obviously true if there exists $\lambda_i \geq 0$, $i = 1, \dots, N$ such that

$$p_0(\cdot) + \sum_{i=1}^N \lambda_i p_i(\cdot) < 0. \quad (22)$$

The above is a version of the S-procedure (Jönsson, 2001) but simplified to static systems- and it is this feature that is utilised in this work to compute the bonds. The benefit of working with (22) is that

it is a linear matrix inequality (LMI) (Jönsson, 2001), a class of well-understood convex problems. For the particular problem considered in the paper, the quantity to be checked $p_0(s, \sigma) < 0$ relates to the quantisation error bound whilst the specified non-negative quadratic constraints characterise properties of the activation functions, inputs sets and quantisation.

Quadratic constraints have a long history in control theory to encode information about unknown nonlinear disturbances (e.g. control saturation (Tarbouriech et al., 2011) and quantisation (Zhou et al., 2010)) within a robustness analysis. For the specific problem considered in this paper, they bring the benefits of a) a common framework for describing the many features of the problem, including the various nonlinearities and sets b) verifying a quadratic constraint can be cast as an LMI – a class of well-studied convex optimisation problems. The two main drawbacks are a) they can lead to conservative bounds as the bounds must hold for all terms satisfying the quadratic algebraic expressions and b) even though an LMI is a convex problem, its complexity scales poorly ($\mathcal{O}(n^6)$ in runtime and $\mathcal{O}(n^4)$ in memory requirements, where n is the number of neurons in the network (Dathathri et al., 2020)). However, the ability to compute worst-case bounds justified its consideration here.

Appendix 4: LMI quadratic constraints for input hyper-rectangle

Each neural network’s input $(x_1, x_2) \in \mathcal{X}$ is assumed to lie within hyper-rectangles.

Definition 2 For the i^{th} neural network with $i \in \{1, 2\}$, define the hyper-rectangle containing the input x_i as $\mathcal{X}_i = \{x_i : \underline{x}_i \leq x_i \leq \bar{x}_i\}$. Within these hyper-rectangles, the combined input data for both NNs is constrained to $(x_1, x_2) \in \mathcal{X}$, with \mathcal{X} potentially capturing cross-conditions relating the two inputs (for example the input of the second NN being the quantised version of the first, $x_2 = q(x_1)$).

The hyper-rectangles \mathcal{X}_i , $i \in \{1, 2\}$ can then be represented by the following quadratic constraints.

Definition 3 For $i \in \{1, 2\}$, if $x_i \in \mathcal{X}_i$ then $\begin{bmatrix} x_i^T & 1 \end{bmatrix} P_{\mathcal{X}_i} \begin{bmatrix} x_i \\ 1 \end{bmatrix} \geq 0$, where

$$P_{\mathcal{X}_i} = \begin{bmatrix} -\lambda_{x_\infty} & \frac{\lambda_{x_\infty}}{2}(\underline{x}_i + \bar{x}_i) \\ (\underline{x}_i + \bar{x}_i)\frac{\lambda_{x_\infty}}{2} & -\underline{x}_i^T \lambda_{x_\infty} \bar{x}_i \end{bmatrix}, \quad \lambda_{x_\infty} \in \mathbb{D}_+^{n_x}. \quad (23a)$$

In addition, if $\bar{x}_1 = \bar{x}_2 = \bar{x}$ and $\underline{x}_1 = \underline{x}_2 = \underline{x}$, then the two inputs (x_1, x_2) also satisfy joint quadratic constraints of the form

$$\begin{bmatrix} (2\bar{x} - (x_1 + x_2)) \\ (\bar{x} - \underline{x}) - (x_2 - x_1) \end{bmatrix}^T P_{\mathcal{X}_{\text{joint}}} \begin{bmatrix} (x_1 + x_2) - 2\underline{x} \\ (x_2 - x_1) + \bar{x} - \underline{x} \end{bmatrix} \geq 0, \quad (24a)$$

where

$$P_{\mathcal{X}_{\text{joint}}} = \begin{bmatrix} \lambda_{x_1+x_2} & 0 \\ 0 & \lambda_{x_1-x_2} \end{bmatrix}, \quad (\lambda_{x_1+x_2}, \lambda_{x_1-x_2}) \in \mathbb{D}_+^{n_x}. \quad (24b)$$

Other joint conditions may also be satisfied by $(x_1, x_2) \in \mathcal{X}$, for instance when the input is quantised $x_2 = q(x_1)$.

$\phi(\cdot)$ property	Sigmoid- $\frac{1}{2}$	tanh	ReLU	ELU	Quantisation	Saturation
Sector bounded	✓	✓	✓	✓	✓	✓
Slope restricted	✓	✓	✓	✓	✓	✓
Bounded	✓	✓	×	×	×	✓
Positive	×	×	✓	×	×	×
Positive complement	×	×	✓	×	×	×
Complementarity condition	×	×	✓	×	×	×
Affine lower bound	×	×	×	×	✓	×
Affine upper bound	×	×	×	×	✓	×

Table 1: Properties of commonly used activation functions, including the sigmoid, tanh, rectified linear unit ReLU and exponential linear unit (ELU).

Appendix 5: LMI quadratic constraints for the activation functions

Definition 4 (Drummond et al. (2020)) Consider a function $\phi(s) : \mathcal{S} \subseteq \mathbb{R} \rightarrow \mathbb{R}$ satisfying $\phi(0) = 0$. This function is said to be sector bounded if

$$\frac{\phi(s)}{s} \in [0, \delta] \quad \forall s \in \mathcal{S}, \quad (25a)$$

slope restricted if

$$\frac{d\phi(s)}{ds} \in [\underline{\beta}, \beta], \quad \forall s \in \mathcal{S}, \quad \beta > 0, \quad (25b)$$

and monotonic if $\underline{\beta} = 0$. If $\phi(s)$ is slope restricted, then it is also sector bounded. The nonlinearity $\phi(s)$ is bounded if

$$\phi(s) \in [\underline{c}, \bar{c}], \quad \forall s \in \mathcal{S}, \quad (25c)$$

is positive if

$$\phi(s) \geq 0, \quad \forall s \in \mathcal{S}, \quad (25d)$$

its complement is positive if

$$\phi(s) - s \geq 0, \quad \forall s \in \mathcal{S}, \quad (25e)$$

and it satisfies the complementarity condition if

$$(\phi(s) - s)\phi(s) = 0, \quad \forall s \in \mathcal{S}. \quad (25f)$$

Lemma 5 Consider $\xi_1, \xi_2 \in \mathbb{R}^M$, where ξ_1, ξ_2 are the arguments of the network activation functions $\phi(\cdot)$ defined in (3). If $\phi(\xi) : \mathbb{R}^M \rightarrow \mathbb{R}^M$ is a sector-bounded nonlinearity then

$$(\xi_i - \phi(\xi_i))^T \lambda_i^{sec} \phi(\xi_i) \geq 0, \quad \lambda_i^{sec} \in \mathbb{D}_+^M, \forall i \in \{1, 2\}. \quad (26)$$

If ϕ is slope-restricted then

$$(\beta(\xi_i - \xi_j) - (\phi(\xi_i) - \phi(\xi_j)))^T \lambda_{i,j}^{slope} (\phi(\xi_i) - \phi(\xi_j) - \underline{\beta}(\xi_i - \xi_j)) \geq 0, \quad \lambda_{i,j}^{slope} \in \mathbb{R}_+^M, \quad \forall (i, j) \in \{1, 2\},$$

and if instead it is just monotonic then

$$(\beta(\xi_i - \xi_j) - (\phi(\xi_i) - \phi(\xi_j)))^T \lambda_{i,j}^{slope} (\phi(\xi_i) - \phi(\xi_j)) \geq 0, \lambda_{i,j}^{mon} \in \mathbb{R}_+^M, \forall (i, j) \in \{1, 2\}. \quad (27)$$

If $\phi(\cdot)$ is positive, then

$$\lambda_i^{pos} \phi(\xi_i) \geq 0, \quad \lambda_i^{pos} \in \mathbb{R}_+^{1 \times M}, \forall i \in \{1, 2\}. \quad (28)$$

If $\phi(\cdot)$ satisfies the complimentary condition, then

$$(\phi(\xi_i) - \xi_i)^T \lambda_i^{cpos} \phi(\xi_i) = 0, \quad \lambda_i^{cpos} \in \mathbb{D}^M \forall i \in \{1, 2\}. \quad (29)$$

Note that (29) is a strict equality condition and that the positivity of the scaling terms λ_i^{cpos} can be relaxed. If both $\phi(\cdot)$ and its complement are positive, then the following cross terms are also obtained

$$\phi(\xi_i)^T \lambda_{i,j}^{crx} (\phi(\xi_j) - \xi_j) \geq 0, \quad \lambda_{i,j}^{crx} \in \mathbb{R}_+^M, \forall (i, j) \in \{1, 2\}, \quad (30a)$$

$$\phi(\xi_i)^T \lambda_{i,j}^{crx, \phi} \phi(\xi_j) \geq 0, \quad \lambda_{i,j}^{crx, \phi} \in \mathbb{R}_+^M, \forall (i, j) \in \{1, 2\}. \quad (30b)$$

Definition 6 (QC for ReLU) If $\phi(\cdot) = \text{ReLU}(\cdot)$ then the matrix Λ in (11) is defined by

$$[\Lambda_{13}, \Lambda_{14}, \Lambda_{15}] = [\lambda_1^{comp}, -\lambda_2^{crx}, -\lambda_2^{cpos}], \quad (31a)$$

$$[\Lambda_{23}, \Lambda_{24}, \Lambda_{25}] = [-\lambda_1^{crx}, \lambda_2^{comp}, -\lambda_2^{cpos}], \quad (31b)$$

$$[\Lambda_{33}, \Lambda_{34}, \Lambda_{35}] = [-\lambda_1^{comp}, \lambda^{crx, \phi} + \lambda_2^{crx} + \lambda_1^{pos}, \lambda_1^{pos} + \lambda_1^{cpos}], \quad (31c)$$

$$[\Lambda_{44}, \Lambda_{45}, \Lambda_{55}] = [-\lambda_2^{comp}, \lambda_2^{pos} + \lambda_2^{cpos}, 0]. \quad (31d)$$

with the scaling terms $\lambda^{crx, \phi}, \lambda_i^{pos}, \lambda_i^{cpos}, \lambda_i^{crx} \in \mathbb{R}_+^{N \times N}, \lambda_i^{comp} \forall i \in \{1, 2\}$ defined in Lemma 5.

Appendix 6: LMI quadratic constraints for quantisation function

Lemma 7 The quantisation function of (9) satisfies the following quadratic constraints: it is sector bounded

$$(x_i - q(x_i))^T \lambda_i^{q, sec} q(x_i) \geq 0, \quad \forall x_i \in \mathcal{X}, i \in \{1, 2\}, \lambda_{sec}^{q, i} \in \mathbb{D}_+^{n_{x_i}}, \quad (32)$$

can be both lower and upper bounded

$$\lambda_i^{q, low} q(x_i) - (x_i - \Delta) \geq 0, \quad \lambda_i^{q, up} (x_i + \Delta - q(x_i)) \geq 0, \quad (33)$$

$$\forall x_i \in \mathcal{X}, i \in \{1, 2\}, (\lambda_i^{q, low}, \lambda_i^{q, up}) \in \mathbb{R}_+^{1 \times n_{x_i}},$$

with these linear bounds implying the following quadratic

$$(q(x_i) - (x_i - \Delta)) \lambda_{i,j}^{q, quad} ((x_j + \Delta) - q(x_j)) \geq 0, \quad \forall (x_i, x_j) \in \mathcal{X}, (i, j) \in \{1, 2\}, \lambda_{i,j}^{q, quad} \in \mathbb{D}_+^{n_{x_i}}. \quad (34)$$

Appendix 7: Proof of Theorem 5

Proof Multiplying (16b) on the right by η and on the left by η^T (defined in (5)) gives

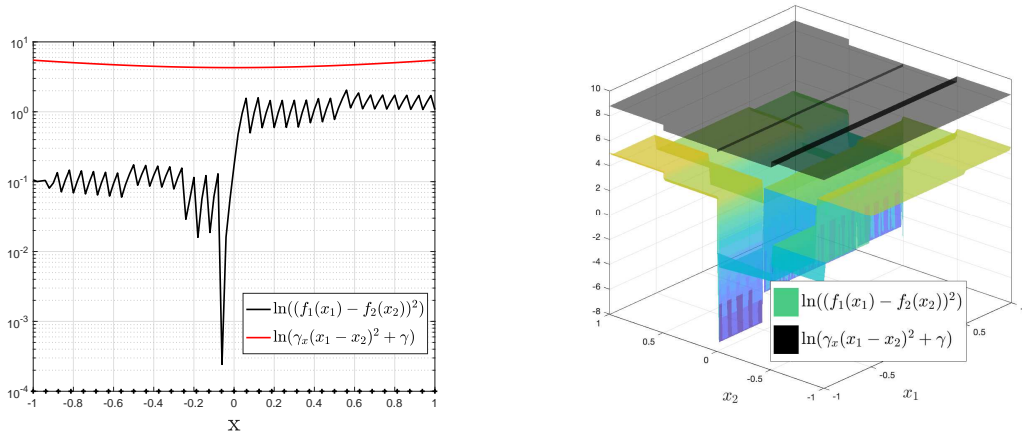
$$M_{\mathcal{X}}(P_{\mathcal{X}}) + M_q(P_q) + M_{\phi}(\Lambda) + M_{\|f-g\|_2}(\Gamma) < 0, \quad (35)$$

where $M_{\mathcal{X}}(P_{\mathcal{X}})$, $M_q(P_q)$ and $M_{\phi}(\Lambda)$ are the non-negative inequalities defined in (10), (13), (11) and where $M_{\|f-g\|_2}(\Gamma)$ is the performance metric defined in (15). Since $M_{in}(P_{\mathcal{X}})$, $M_q(P_q)$ and $M_{\phi}(\Lambda)$ are non-negative whenever $x \in \mathcal{X}$, then for (35) to hold, it must be that $M_{\|f-g\|_2}(\Gamma) < 0$, giving the bound of (17). ■

Appendix 8: Numerical experiment tables and figures

ℓ	γ_x	γ	mean(T)	max(T)	min(T)	Run time (s)
1	24.8575	57.2894	2.5159	13.1337	0.6822	0.8756
2	238.8581	480.2185	3.0544	11.9611	1.3480	3.7339
3	2691.6	3906.6	3.6554	11.2762	1.9924	18.6808
4	23887	36349	4.8567	13.5523	3.1687	80.9595

Table 2: Average values (over 100 runs) of key data for neural network comparison error bounding via SDP, $T = \ln(f_1(x_1) - f_2(x_2))^2) - \ln(\gamma_x(x_1 - x_2)^2 + \gamma)$.



(a) A typical quantisation error bound with $\Delta = 2^{-3}$ and $\ell = 2$. Marks at the bottom of the figure indicate the quantisation steps.

(b) A quantisation error bound in 3D $\Delta = 2^{-1}$ and $\ell = 3$.

Figure 4: Quantised neural network error bound in 3D.

ℓ	γ_{x_1}	γ	mean(T)	max(T)	min(T)	Run time (s)
1	0.5562	0.1091	3.2032	9.5861	1.2384	0.8431
2	2.8599	10.4683	4.1161	10.3115	2.0622	3.2660
3	44.5753	142.9811	5.0260	10.7227	2.9576	17.4438
4	714.7888	1855.4	5.9266	11.0908	3.9657	81.2052

Table 3: Average values (over 100 runs) of key data for quantisation error bounding via SDP, $T_q = \ln(f(x_1) - f_2(x_2))^2) - \ln(\gamma_{x_1}x_1^2 + \gamma)$.

FB	γ_{x_1}	γ	mean(T)	max(T)	min(T)	Run time (s)
1	26.5297	116.6794	3.8375	9.3110	1.8663	3.3577
2	9.4497	45.1156	3.8406	9.7291	1.7572	3.2531
3	3.5685	14.1498	4.0627	10.0648	1.9062	2.8566
4	1.0917	4.3742	4.2453	10.3294	2.1122	3.1510
5	0.2653	1.0961	4.4950	10.9553	2.2159	3.2101

Table 4: Average values (over 100 runs) of key data for quantisation error bounding via SDP for various quantisation levels, $T_q = \ln(f(x_1) - f_2(x_2))^2) - \ln(\gamma_{x_1}x_1^2 + \gamma)$.

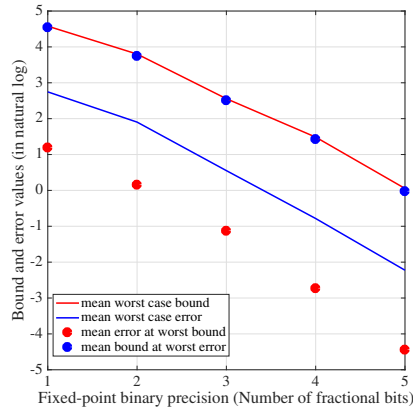
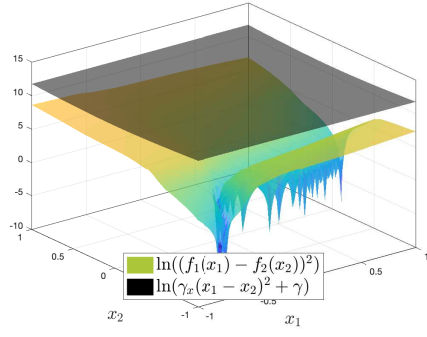
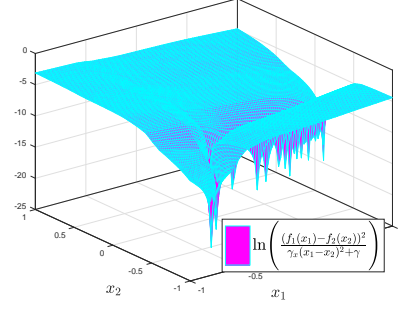


Figure 5: Progression of worst case bound and error with quantisation level $\ell = 2$.



(a) The error (coloured) and bound (grey) surfaces.



(b) The tightness surface T of the bound and error surfaces in Fig. 6(a), viewed from another angle.

Figure 6: Example pruned neural network comparison bound with $\ell = 4$.